Considerations for Post-processing Parameters in Mixed-Method 3D Analyses

A Mesolithic Mandibular Case Study

Robert Z. Selden Jr., *Lauren N. Butaric*, *Kersten Bergstrom*, *and Dennis Van Gerven*

ABSTRACT

The production of three-dimensional (3D) digital meshes of surface and computed tomographic (CT) data has become widespread in morphometric analyses of anthropological and archaeological data. Given that processing methods are not standardized, this leaves questions regarding the comparability of processed and digitally curated 3D datasets. The goal of this study was to identify those processing parameters that result in the most consistent fit between CT-derived meshes and a 3D surface model of the same human mandible. Eight meshes, each using unique thresholding and smoothing parameters, were compared to assess whole-object deviations, deviations along curves, and deviations between specific anatomical features on the surface model when compared with the CT scans using a suite of comparison points. Based on calculated gap distances, the mesh that thresholded at "0" with an applied smoothing technique was found to deviate least from the surface model, although it is not the most biologically accurate. Results have implications for aggregated studies that employ multimodal 3D datasets, and caution is recommended for studies that enlist 3D data from websites and digital repositories, particularly if processing parameters are unknown or derived for studies with different research foci.

Keywords: archaeoinformatics, computational archaeology, geometric morphometrics, digital humanities, museum studies

La producción de mallas digitales tridimensionales (3D) de superficie e información tomográfica computarizada (TC) se ha generalizado en los analisis morfométricos de datos antropológicos y arqueológicos. Dado que los métodos de procesamiento no están estandarizados quedan dudas sobre la comparabilidad de conjuntos de datos 3D procesados y curados digitalmente. El objetivo de este estudio fue identificar los parámetros de procesamiento que tienen la compatibilidad más consistente entre mallas derivadas de TC y un modelo de superficie 3D de la misma mandibula humana. Fueron comparadas ocho mallas cada una con parámetros únicos de umbralización y suavizado, para evaluar las desviaciones de todo el objeto, las desviaciones a lo largo de las curvas y las desviaciones entre características anatómicas específicas en el modelo de superficie, en comparación con cada una de las tomografías computarizadas utilizando un conjunto de puntos de comparación. Con base en las distancias de separación calculadas, aunque no las más precisas desde el punto de vista biológico, se encontró que la malla con umbral en "0" con una técnica de suavizado aplicada se desvía menos de la superficie modelo. Los resultados tienen implicaciones para los estudios agregados que emplean conjuntos de datos 3D multimodales y se recomienda precaución para los estudios que incluyen datos 3D de sitios web y repositorios digitales, especialmente si los parámetros de procesamiento son desconocidos o derivados de estudios con diferentes focos de investigación.

Palabras clave: arqueoinformática, arqueología computacional, morfometría geométrica, humanidades digitales, estudios de museo

Analyses of three-dimensional (3D) data are increasingly widespread in paleoanthropology, bioanthropology, bioarchaeology, and archaeology (Adams et al. 2013; Friess 2012; Shott 2014; Slice 2007; Tocheri 2009). With advances in virtual anthropology (for a review, see Weber 2015), studies have begun to stray from traditional linear methods (e.g., caliper distances), and 3D data collection methods are regularly employed to include surface scanning (laser, structured light, etc.), computed tomographic (CT) imaging (Franklin et al. 2016), and MicroScribe data (Menéndez 2017). The fusion of traditional and geometric morphometrics is similarly a topic of considerable interest (Robinson and Terhune 2017).

Three-dimensional data exhibit several advantages over traditional caliper measurements. For instance, CT imaging captures data associated with internal structures (e.g., paranasal sinuses; Butaric 2015; Rae and Koppe 2002) or diploë/trabecular bone patterning

Advances in Archaeological Practice 9(4), 2021, pp. 325–337

DOI:10.1017/aap.2021.18

(e.g., Chirchir et al. 2017; Copes and Kimbel 2016). Advanced geometric morphometric methods can be applied to any 3D mesh, in some cases capturing more variation with shape data compared to linear measures (Bookstein et al. 2004; Gunz and Mitteroecker 2013). Distorted and/or fragmentary fossils and cultural materials can be virtually reconstructed prior to analysis (Balzeau et al. 2010; Godinho and O'Higgins 2017; Gunz et al. 2009; White 2015; Zollikofer and Ponce de Leon 2005). Those data associated with scanned objects can be digitally curated for future use and shared through digital repositories (e.g., MorphoSource, Open Science Framework [OSF], GitHub, Figshare, Zenodo, the Open Research Scan Archive [ORSA], Open Context, the Digital Archaeological Record [tDAR], or virtual museum collections; Bruno et al. 2010; Isler et al. 2006; Kuzminsky and Gardiner 2012; Selden et al. 2020, 2021; Selden, Perttula et al. 2014; Shearer et al. 2017).

The latter point is of particular interest because it minimizes the need to handle fragile specimens, saves time and fiscal resources for researchers and museum/collection personnel, fosters the advancement of next-generation research through ease of sharing, encourages collaboration among researchers and institutions, and can increase accessibility to the general public (Allison 2008; Douglass et al. 2017; Means 2015, 2017; Selden, Means et al. 2014; Wachowiak and Karas 2013; Weber 2015). Virtual databases have allowed for the continuation of research during the COVID-19 pandemic, during which time museum travel—and travel in general—has largely been limited or restricted. It stands to reason that as the number of data-sharing endeavors increases, efforts to incorporate 3D data collected and processed using different modalities will increase as well. When mixing digitally rendered meshes generated from CT and surface scan data—or even different scanners within the same modality, such as between different 3D laser scanners—the question of whether those meshes are directly comparable is of considerable importance.

Consequently, numerous studies have investigated quality control and reliability by comparing digital and linear measures taken using various modalities (Fourie et al. 2011; Stephen et al. 2015; Stull et al. 2014). For example, when comparing CT and traditional caliper-collected data among skeletal studies, linear distances obtained from CT scans were found to be as reliable as those collected by hand (Koppe and Nagai 1995; Koppe and Schumacher 1992; Márquez and Laitman 2008; Montgomery et al. 1979; Zonneveld et al. 1989). Similar results have been undertaken to compare caliper measures to data collected with MicroScribes (Menéndez 2017; Stephen et al. 2015) and laser scanners (Evgenikou and Georgopoulos 2015). Additional studies have investigated inter-methodological reliability in the collection of landmarks and distances among different sources (Algee-Hewitt and Wheat 2016; Katz and Friess 2014; Shearer et al. 2017; Sholts et al. 2011; Tzou et al. 2014). For example, Robinson and Terhune (2017) tested both inter-observer and inter-method error rates in a mixed-method study. Even though they specifically found that inter-method error rates overlapped with normal levels of variance among their samples, the authors cautioned researchers when using data compiled from multiple observers and technologies.

Although they are informative for a wide range of methodological techniques, analyses rarely investigate or discuss the importance of differential post-processing. Even though Robinson and Terhune (2017:64) were exhaustive in capturing inter-observer and inter-method error rates using four data collection methods to analyze variance at multiple levels, the details of their post-processing techniques are scarce. Furthermore, they mention that when processing microCT data, the "thresholding tool was employed to remove extraneous material from the scans [and was] manually adjusted until only bone [was] selected" (Robinson and Terhune 2017:64). Although they assume this subjective method would not have a significant impact on the morphology of the external surface bone, it was conceded that differences in the effect of thresholding settings are worthy of further investigation (Robinson and Terhune 2017:64).

More recently, Stock and colleagues (2020) investigated the effects of different processing techniques in segmentation of CT scans when modeling human pelvic bones. Ultimately, these authors noted that a small degree in varying threshold levels do not significantly alter measures on the 3D models. More important, they found that a consistent methodological approach across observers for segmentation and smoothing techniques is essential for precise data collection. They further note the need for additional error-based studies to test for quality control in using digitally derived data.

This investigation builds on recent efforts to explore variation introduced by different modalities of 3D scanners (Shearer et al. 2017), and the purpose of the current study is to assess whether meshes generated by CT and surface scanners can be pooled together for mixed-method studies as a means of increasing sample sizes—and if so, whether specific post-processing techniques should be followed. Given that several recent studies investigate inter-observer and inter-method error rates using linear dimensions (for a recent review, see Robinson and Terhune 2017), we focus solely on post-processing techniques of 3D data.

METHODS

This study focused on post-processing techniques for a single object using two primary 3D data-capturing technologies: CT and surface (structured light) scans. The specimen used in the analysis is a mandible from the Mesolithic Wadi Halfa Collection (B11-2-15904). Original data collection involved CT and surface scanning of the Wadi Halfa Collection for a larger, ongoing project investigating the evolutionary craniofacial changes of these individuals and neighboring populations. During the development of that larger project, questions regarding mixed-modalities in image processing developed, leading to the current project. This mandible, versus other cranial bones, was chosen for the current study based on its complex geometry (including a broken condyle) and varying matrix densities (bone vs. enamel), which may impact CT-processing techniques.

The Wadi Halfa remains, as represented by the mandible presented here, were excavated with the full support of the Sudanese government from 1963 to 1964. This excavation was funded by the then largest international (UNESCO) salvage program ever assembled. Following its recovery and subsequent analyses, the osteological material was safely and securely housed at University of Colorado Boulder, where only qualified scholars were allowed access to it. In 2018, the Wadi Halfa Mesolithic collection was moved to Arizona State University, where it is housed today. For extensive background information on the collection and excavation, see Greene and Armelagos (1972).

https://doi.org/10.1017/aap.2021.18 Published online by Cambridge University Press

TABLE 1. Isosurface Thresholds Used in the Analysis.

Mesh	CT Threshold	Smoothed?	Description
M1	0	Yes	midpoint thresholding; Amira default
M2	0	No	
M3	−500	Yes	based on subjective viewing[a]
M4	−500	No	
M5	562	Yes	HMH thresholding based on mandible body-air boundary
M6	562	No	
M7	634	Yes	HMH thresholding based on the enamel-air boundary
M8	634	No	

[a] Removed underlying towel and artifacts while keeping object visible.

CT Scanning and Processing

Scanning of the mandible was conducted at the Department of Radiology, Anschutz Medical Campus of University of Colorado Denver, using a Philips Gemini TF TOG 64 CT scanner with the following parameters: kVp140 mA30, 152FOV, and 0.625 mm slice thickness. Resulting files were saved as 16-bit DICOMs using VGStudio 2.2.

Although often ignored (for an exception, see Stock et al. 2020), post-processing is a particularly important step in the analysis of CT images. Several studies have demonstrated that selecting the appropriate window level and thresholding technique is vital for creating accurate 3D models of the original item (Schwartz et al. 1998; Spoor et al. 1993; Ullrich et al. 1980). There are various parameters and steps associated with CT post-processing that are dependent on material type (for step-by-step reviews, see Spoor et al. 2000; Weber and Bookstein 2011). As a result, scanning parameters may differ if one is investigating bony elements versus denser elements such as enamel or fossil matrix. This process is further confounded when analyzing an object with mixed materials, such as crania and mandibles that contain both bone and enamel. Additional post-processing of the mesh involves the decision to apply a smoothing factor (or not), to simplify the mesh (or not) to reduce the number of poly-faces in the mesh, and to remove additional artifacts (or not) from the mesh.

A total of eight isosurface meshes were rendered from the CT scan data in Amira 5.6 (Stalling et al. 2005) using different post-processing techniques (Table 1). Differences in mesh creation were based on variable threshold levels and the application, or not, of a smoothing technique. CT images are represented by 3D stacks of pixels—that is, voxels, where varying shades of gray related to the degree of radiation intensity are assigned numeric values called Hounsfield units. In most cases, materials with the lowest densities (typically air) appear as darker grays or black and are represented by low numeric values, whereas materials with higher densities (e.g., bone, enamel, fossilised matrix, etc.) are usually lighter gray to white and are represented by higher numeric values (Prossinger et al. 2003; Spoor et al. 2000). The lighter gray and white values of bone are not always easy to distinguish from the darker gray and black values of air. This is because slightly varying shades can be challenging for the human eye to decipher, resulting in blurred versus sharp air-to-bone (or other material) boundaries (Weber and Bookstein 2011).

Subjectively deciding where the air-to-bone boundary exists can result in artificial size differences among CT scan data. Therefore, the first step in creating accurate 3D meshes is to identify air versus the object in question (e.g., bone, rock/clay, etc.) through establishing a thresholding parameter. A higher threshold number results in less of the object being rendered (creating artificially thin areas and/or holes), whereas a lower threshold number results in more aspects of the object being rendered (perhaps artificially bloating or increasing the size of the object). To address this, the half-maximum-height (HMH) technique was previously developed to determine this boundary objectively (Schwartz et al. 1998; Spoor et al. 1993; Ullrich et al. 1980). This technique averages the minimum and maximum values for the CT number across the boundary in question (e.g., air-bone, enamel-dentin). The number —essentially the midpoint value—is used to discriminate between air and bone, or other materials of interest, objectively. Consequently, when creating a mesh, all voxels corresponding to that threshold parameter will remain in the mesh, whereas voxels lower than that number will effectively be removed.

Four thresholding techniques were applied to create isosurfaces in Amira, using the isosurface tool. An isosurface represents a mesh of polygons that corresponds to grayscale values within the set thresholding parameters. It is important to note that, much like in surface scanning, isosurfaces only render external elements of the object. For meshes 1 and 2 (abbreviated as M1 and M2 in Table 1) a neutral threshold value of 0 was used so that any voxel lower than 0 was not rendered into the isosurface. This is the random, default setting in Amira. For meshes 3 and 4 (M3, M4) a threshold of −500 was applied. This threshold was subjectively determined in Amira to remove the underlying towel and CT-scanner bed (lower density objects) on which the mandible rested, while keeping the mandibular elements visible. The remaining two thresholding parameters for meshes 5–8 (M5–M8) were determined using the HMH technique. To identify the appropriate HMH numbers, the CT scan was uploaded to ImageJ 1.50i (http://imagej.nih.gov/ij/), where the maximum and minimum gray values were recorded using the line-measurement tool, following several studies (Butaric 2015; Coleman and Colbert 2007). First, 20 measurements were collected across the mandibular bone-air transition and averaged to obtain an HMH value appropriate for bone (M5, M6). Then, 20 measurements were collected across the enamel-air boundary and averaged to obtain an HMH value appropriate for enamel (M7, M8). These HMH values were used to create two additional isosurfaces in Amira. Following the

https://doi.org/10.1017/aap.2021.18 Published online by Cambridge University Press

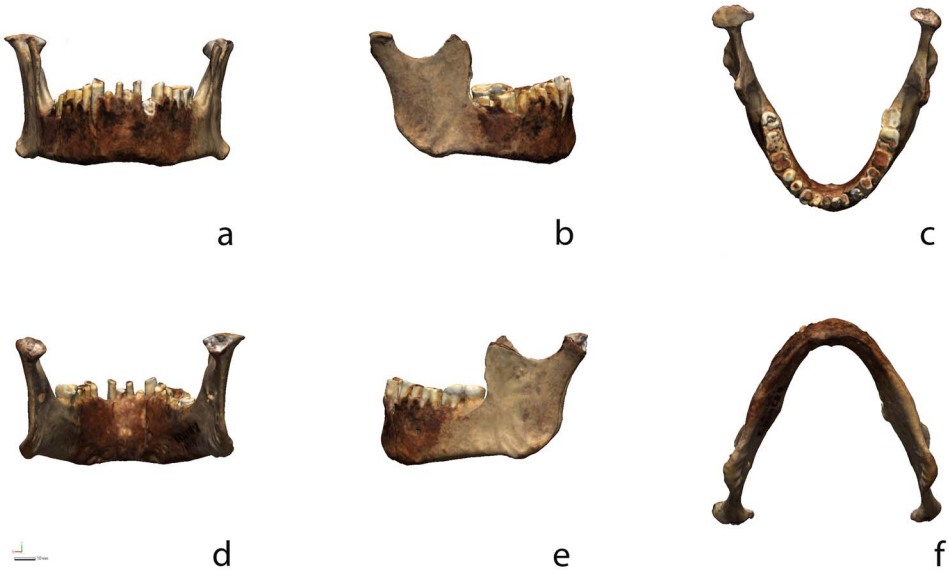

FIGURE 1. Surface scan data (with texture) for Mesolithic mandible B11-2-15904 from the Kulubnarti collection illustrating (a) anterior, (b) right buccal, (c) superior, (d) posterior, (e) left buccal, and (f) inferior views. The full-size figure can be viewed and downloaded at GitHub, and the 3D mesh generated by the surface scanner can be viewed interactively on Sketchfab.

creation of the four isosurfaces, the generate surface tool in Amira was applied to each, and all four meshes were exported as a stereolithographic file (.stl) for the analyses.

Copies of these meshes were also subjected to the smoothing tool in Amira (four iterations, lambda 0.9), reducing the noise between the mesh poly-faces. The four smoothed meshes were exported as.stl files, resulting in a total of eight comparative meshes (Table 1). All meshes were subsequently imported into Geomagic Studio 2014 (3D Systems Inc.) to remove additional artifacts produced during processing and to address issues associated with folded/non-manifold poly-faces and small tunnels/holes. To ensure that processing across the models remained objectively the same at this step, the *Mesh Doctor* function was used to automate the process. These eight models comprise the test.

Surface Scan Processing and Modeling

In addition to the CT scans, the mandible (B11-2-15904) was also scanned with a Creaform GoSCAN 20. Following scanner optimization and shutter-speed configuration, scan data were collected atop a flat turntable at a 0.1 mm resolution with positioning targets required for increased accuracy. The mesh was cleaned in VXmodel 8.1.1, ridding it of isolated patches, self-intersections, spikes, small holes, singular vertices, creased edges, narrow triangles, outcropping triangles, narrow bridges, and non-manifold triangles. The point cloud associated with the unprocessed scan data was saved and exported as an.stl file prior to post-processing (Weyrich et al. 2004).

Surface scan data (Georgopoulos et al. 2010; Mahmoud et al. 2015) were subsequently imported to Geomagic Design X (Dx), where an additional check for mesh errors was used to address potential issues with non-manifold poly-vertices, folded poly-faces, dangling poly-faces, small clusters, small poly-faces, non-manifold poly-faces, crossing poly-faces, and small tunnels. Due to the limitations of surface scanning, areas of the mesh associated with the mental foramina were cut, and the mesh boundary was edited prior to alignment. Following alignment, scan data were saved, and an object file (.obj) was exported for use as a 3D figure (Figure 1).

Following data collection, the mandible was modeled in Dx using a custom patch network designed to capture the detail of the mesh in a surface model. Three-dimensional contour curves were applied along high curvature areas that were used as the basis for the initial layout of the custom patch network. The first iteration of the patch network enlisted an auto estimation for the number of patches necessary, which was subsequently refined through a series of iterative comparisons between the surface model and the mesh by moving between Dx and Geomagic Control X (Cx).

Throughout the design and layout process for the patch network, each iteration of the freeform surface model was exported to Cx to identify areas of the surface model's design that exceeded the specified—arbitrary—tolerance (0.1 mm, the same as post-processed mesh resolution) and required revision. Development of the final surface model was an iterative process resulting in a total of three revisions, yielding a freeform surface model where 100% of the surface model is within the 0.1 mm tolerance of the mesh. Revisions to the custom patch network were conducted by shuffling patch groups, editing, and inserting splines. The final freeform surface model was then exported to Cx for comparisons with the processed CT-rendered model. Although surface scan data were used as the control, that is not meant to convey a measure of accuracy or precision. Instead, these data are used to identify the CT post-processing method that yields a mesh with the smallest deviation between the surface model and CT-generated data.

https://doi.org/10.1017/aap.2021.18 Published online by Cambridge University Press

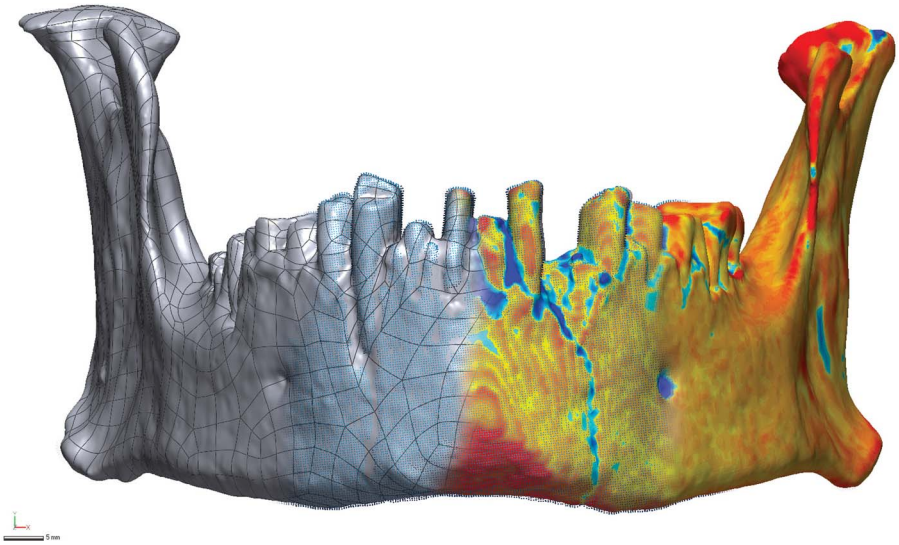

FIGURE 2. Surface model (left) contrasted with CT point cloud (center) and gap distances between the surface model and CT mesh (right). Inspection tolerance was altered to 0.05 mm to more dramatically illustrate deviations that occur between the mesh and surface model for this figure. The full-size figure can be viewed and downloaded at GitHub.

Computer-Aided Inspection

Cx was used to compare the topology of the surface model (nominal data) against that of the eight CT meshes (measured data; Selden 2017; Selden and Jones 2021; Figure 2). Measured data was compared against the nominal data (Li and Gu 2004; Minetola et al. 2015; Obeidat and Raman 2008; Poniatowska 2012) to identify the method of CT post-processing that best fits with the surface model based on the percentage of the 3D mesh that meets with a prespecified—arbitrary—tolerance (0.3 mm; Budzik et al. 2016; Wong et al. 2006; Yogi et al. 2014). Once identified, a series of two-dimensional (2D) slices were generated for the CT mesh that best fit with the surface scan to further clarify the character of the geometric shapes associated with gap distances.

A total of 33 reference points were populated on the mesh in Dx (Figure 3). These points were placed in the vicinity of mandibular landmarks (e.g., menton) and were selected specifically due to their use in an unrelated study of the Mesolithic Kulubnarti mandibles (Galland et al. 2016). The reference points were saved as an initial graphics exchange specifications (IGES) file and imported to Cx as comparison points, where they were used to assess deviations between the surface model and CT meshes at known locations of analytical importance. Note that comparison points associated with the fractured left condyle of the mandible were not reflected here because they were in the geometric morphometric study (Galland et al. 2016). A number of methods have been proposed to reconstruct (Benazzi et al. 2009; Senck et al. 2015) or otherwise account for missing data in geometric morphometrics (Arbour et al. 2014; Couette and White 2010; Neubauer et al. 2012; Senck et al. 2013; Zelditch et al. 2012), none of which were used here. Instead, comparison points were placed atop the area of the fracture, which afforded an opportunity to explore how a region of highly variable geometry would compare between the surface model and the CT meshes.

RESULTS

Comparisons are limited to the topology of the surface model due to the fact that it is not possible to capture interior structures with a surface scanner. It is, however, possible to compare the topology of the CT mesh against that of the surface scan by limiting the analysis to the topology of the surface model.

Mesh Comparison (3D Compare)

The 3D comparisons of the surface model across the eight CT meshes suggest that the M1 HMH 0 smooth mesh (in tolerance [InTol] 93.92%) and the M2 HMH 0 mesh (InTol 93.80%) correlate best with the surface model when the entirety of the mandible geometry—100% sampling ratio—is compared (Table 2). CT meshes M3 and M4 HMH −500 smooth and HMH −500 demonstrate the lowest tolerance levels (InTol 62.20% for both), so they correspond least to the surface scan. Additional comparisons indicate that high gap distances occur primarily in regions between dentition and around the mental foramina. Deviations also occur on the anterior rami and condyles, particularly in the area of the fractured left condylar neck (Figure 4).

The histogram in Figure 4 illustrates the Gaussian distribution for the number of errors over the whole deviation. The graph is split into six segments: 1σ at 31% from the average to the maximum deviation in each direction, 2σ at 69% from the average to the maximum deviation in each direction, and 3σ at 93.3% from the average to the maximum deviation in each direction. The average (AVG) is the sum of all deviations divided by the number of all deviations, and the RMS is the square root of all squared deviations divided by the number of all deviations (sometimes referred to as the "effective deviation"). In tolerance (InTol) and out tolerance (OutTol) percentages indicate the percentage of deviations in or out of the given tolerance, and over tolerance (OverTol) and under tolerance (UnderTol) percentages indicate the

https://doi.org/10.1017/aap.2021.18 Published online by Cambridge University Press

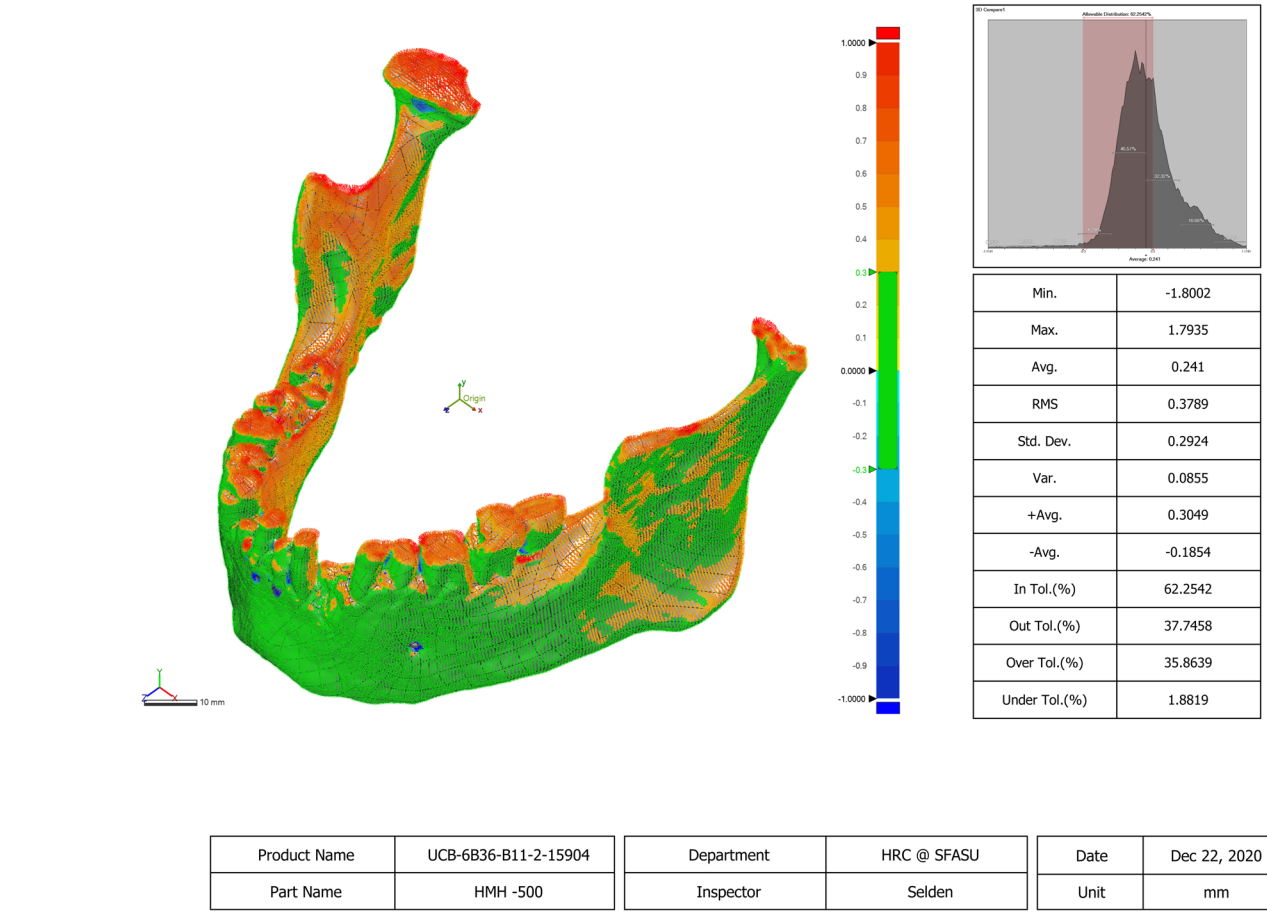

FIGURE 3. Location of the 33 landmarks used in Galland and colleagues (2016; Supplemental Data), which were populated on the surface model in Dx and imported as comparison points to Cx. The full-size figure can be viewed and downloaded at GitHub.

TABLE 2. Results of 3D Comparison between Surface Scan and CT Meshes.

CT Mesh	InTol (%)	OutTol (%)	OverTol (%)	UnderTol (%)
M1	93.9161	6.0839	3.3545	2.7294
M2	93.8012	6.1988	3.4278	2.7710
M3	62.1989	37.8011	35.7474	2.0537
M4	62.2542	37.7458	35.8639	1.8819
M5	90.5318	9.4682	8.6902	0.7779
M6	88.3977	11.6023	10.8934	0.7090
M7	87.4393	12.5607	11.9468	0.6139
M8	87.4647	12.5353	11.8925	0.6428

percentage of deviations over (positive direction) or under (negative direction) the tolerance range.

2D Sectioning (2D Compare)

The 2D comparison was generated for four sections of HMH 0 smooth at or very near locations on the mesh where comparison points—based on landmarks used by a previous study—were later applied (Table 3). Each section articulates with a specific curve, where semilandmarks (equidistant or otherwise) might be applied. For each of the 2D compare sections, two call-outs were added to illustrate the maximum measures of over/under tolerance. The single exception to the call-outs occurs in 2D compare 3, where gap distances associated with the mental foramina were of interest. In the case of 2D compare 3, the call-outs were issued for the two highest deviations that occur under the ± 0.3 mm tolerance.

Through sectioning the specific CT mesh found to best fit the surface scan, variation between the surface scan and the HMH 0 smooth mesh was calculated. Even in the most ideal cases, some areas of the mesh may not be well suited for semilandmarks. For example, it would take substantial effort to identify areas of the left fractured condylar neck, left anterior ramus, left mandibular foramen, and both mental foramina where landmarks and semilandmarks would be deemed acceptable for inclusion in a formal analysis. However, a number of other areas remain on the HMH 0 smooth mesh that are likely suitable for use in a mixed-method analysis, but final placement would be dependent on the specifics of the research question.

https://doi.org/10.1017/aap.2021.18 Published online by Cambridge University Press

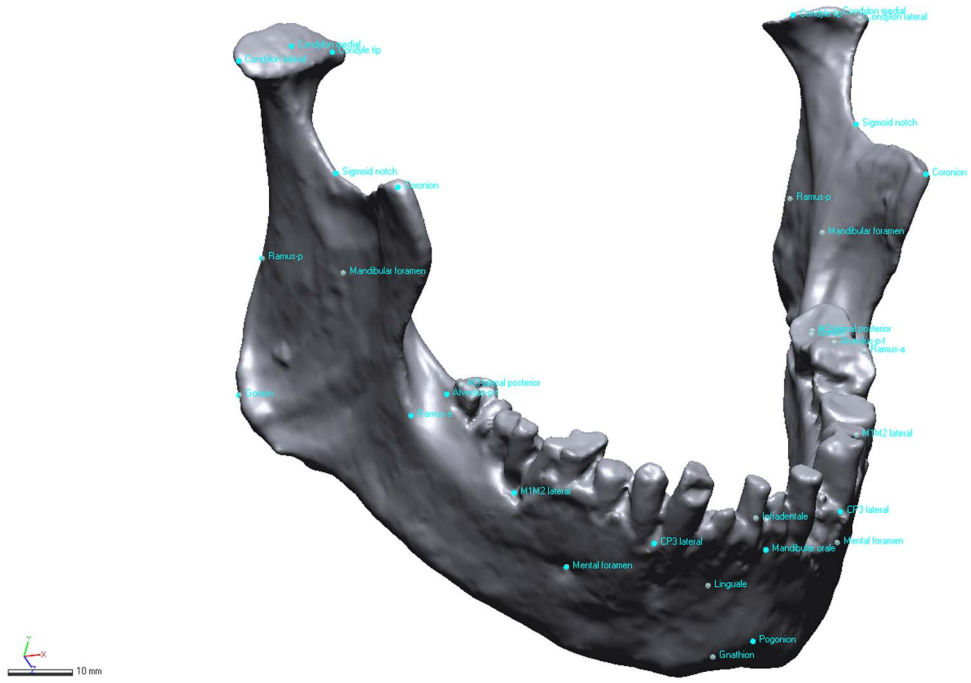

FIGURE 4. Comparison between the surface model and the thresholding methods (isosurfacing) for HMH 500 (M4). Regions of mesh topology in green represent the geometry of Mesolithic mandible B11-2-15904 within the ± 0.3 mm tolerance. 3D comparison results associated with the HMH 500 smooth (M3) and HMH 500 (M4) meshes exhibited the highest deviations from the surface model. The full-size figure can be viewed and downloaded at GitHub.

TABLE 3. Results of Sectioning (2D Compare) for HMH 0 Smooth in High-Deviation Regions of the Surface Scan / CT Mesh near the Locations of Landmark Data.

2D compare	InTol (%)	OutTol (%)	OverTol (%)	UnderTol (%)
2D compare 1	56.2259	43.7741	41.7202	2.0539
2D compare 2	88.5312	11.4688	4.8290	6.6398
2D compare 3	93.9781	6.0219	0.6691	5.3528
2D compare 4	80.0948	19.9052	14.2180	5.6872

Comparison Points

Figure 3 illustrates the placement of comparison points, and Figure 5 demonstrates the gap distance for comparison points between the surface model (reference position) and each of the eight meshes (measured position) in Cx. Gap distances were recorded (Table 4; Supplemental Data), and results are listed in order for the eight post-processing methods. Comparison points placed on the gnathion, gonion, and pogonion showed low (in tolerance) gap distances, whereas other anatomical regions demonstrated gap distances that were above tolerance for at least one of the CT meshes.

Comparison points placed around landmarks across the different CT meshes did not correspond well, with several exhibiting gap distances above the ± 0.3 mm tolerance. The CT meshes that best correspond with the repurposed constellation of comparison points were M1 and M2 (HMH 0 smooth and HMH 0). For these meshes, only three comparison points extend beyond the ± 0.3 mm tolerance: condylon tip (L), condylon medial (L), and mental foramen (L). It is important to reiterate, however, that the two measures atop the left condyle were collected in the area of a fracture, so this result is not unexpected (see discussion below). The meshes displaying the highest gap distances were the M3 and M4 CT meshes (HMH −500 smooth and HMH −500). It is worth noting that although mesh topology for M3 and M4 does vary in terms of the 3D compare analyses, gap distances for comparison points were exactly the same. Results for the M5–M8 meshes are also similar in terms of which landmarks extended beyond the median and maximum tolerance. In total, four landmarks remain below the median tolerance for *all* meshes (pogonion, gnathion, gonion [R], and gonion [L]), and only one landmark included a gap distance reaching only the median tolerance (ramus-a [R]). For the remainder of the comparison points, at least one extended beyond the maximum tolerance for all CT meshes (Table 4).

DISCUSSION

Eight CT meshes were digitally rendered using different thresholding parameters, then compared to a single 3D surface model to identify the post-processing method for CT scans that produces the smallest gap distances in terms of surface topology (3D comparisons), the sections most suitable for landmark and/or semilandmark placement (2D section comparisons), and the smallest gap distances in terms of landmark placement (comparison point analyses). All three analyses demonstrate that post-processing methods impact the comparability of the 3D meshes that are the primary data source used in studies of 3D geometric morphometrics. Consequently, if one is conducting a mixed-

https://doi.org/10.1017/aap.2021.18 Published online by Cambridge University Press

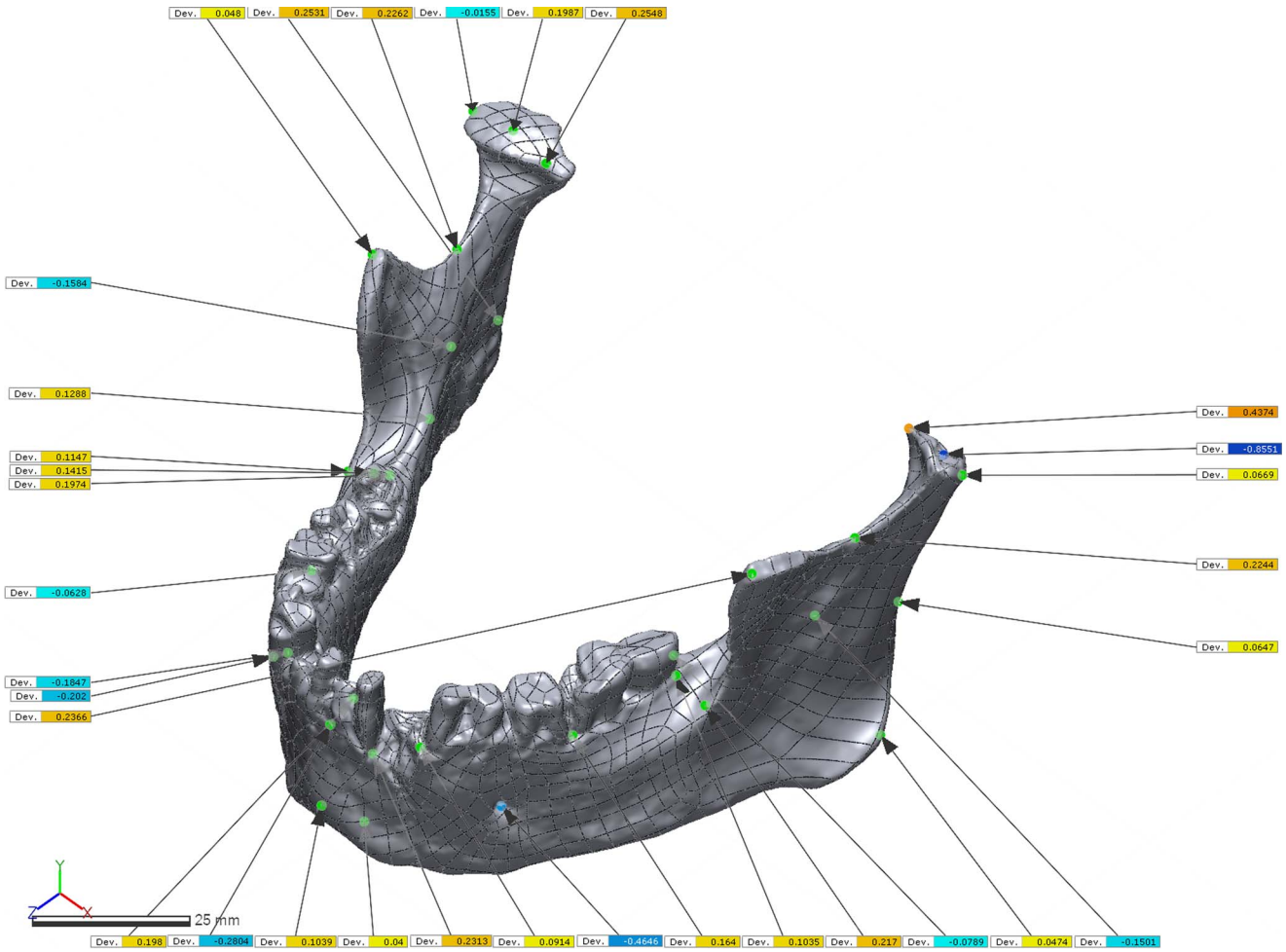

FIGURE 5. Surface model and comparison points contrasted with CT mesh HMH 0, illustrating the locations for measured positions and gap vectors associated with locations used in an unrelated geometric morphometric analysis (Galland et al. 2016; Supplemental Data). Green points denote a comparison point within tolerance; yellow points indicate a comparison point within tolerance, but above/below ± 0.15 mm; and red/blue boxes indicate a comparison point beyond the ± 0.3 mm tolerance. Importantly, these are not landmark-to-landmark measures; instead, they reflect the gap distance between the surface model and CT mesh at the location of the comparison point on the surface model. The full-size figure can be viewed and downloaded at GitHub.

method study, incorporating those analyses employed here would be beneficial to identify which post-processing techniques yield the most consistent mixed-method dataset needed to address a specific research question while also highlighting those aspects of mesh geometry most suitable for landmark and semilandmark application in more advanced studies. As detailed below, it is recommended that unprocessed data be made available in addition to processed 3D meshes, making it possible to achieve consistent data processing for studies where reuse is possible, as well as replication studies where the processed mesh can be used.

Mesh Comparison (3D Compare)

Results indicate that the neutral CT-mesh M1, HMH 0 smooth, is the best match to the surface model in terms of overall model composition; however, this result does not necessarily mean that the HMH 0 smooth mesh is the most biologically accurate. As mentioned previously, numerous studies (Schwartz et al. 1998; Spoor et al. 1993; Ullrich et al. 1980) have demonstrated that post-processing techniques, which include the HMH technique for objectively determining appropriate thresholding values depending on the material involved, are extremely important for obtaining accurate models and measurements. Despite this, studies enlisting CT meshes continue to use subjective methods and/or do not provide additional processing information.

It is likely that the appropriate post-processing methods for one study will not translate across multiple studies, given that research interests tend to be wide ranging. With this in mind, it is recommended that researchers pay particular attention when selecting the appropriate processing method. If mixed-method data cannot be avoided, preliminary comparative analyses that contrast results

https://doi.org/10.1017/aap.2021.18 Published online by Cambridge University Press

TABLE 4. Gap Distances between Points at Landmarks Applied to the Surface Scan Contrast with the Post-Processed CT Meshes.

CMP1	M1	M2	M3	M4	M5	M6	M7	M8
Infradentale	*0.2102*	*0.1980*	**0.8376**	**0.8376**	0.0177	0.0040	–0.0327	–0.0380
Pogonion	0.1039	0.1039	0.1391	0.1391	–0.0285	–0.0284	–0.0444	–0.0440
Gnathion	0.0492	0.0400	0.0282	0.0282	–0.0968	–0.1175	–0.1226	–0.1388
Mandibular orale	**–0.3123**	*–0.2804*	*–0.1671*	*–0.1671*	**–0.8656**	**–1.4265**	**–0.8968**	**–0.8860**
Condylon lateral (R)	0.0018	–0.0155	*0.2077*	*0.2077*	*–0.2104*	*–0.2174*	**–0.3048**	*–0.2231*
Condylon medial (R)	*0.1970*	*0.1987*	**0.8456**	**0.8456**	0.0359	0.0212	0.0175	0.0028
Condylon tip (R)	*0.2646*	*0.2548*	**0.7939**	**0.7939**	0.1371	0.1328	0.1113	0.1114
Condylon tip (L)	**0.3994**	**0.4374**	**0.6508**	**0.6508**	*0.2929*	**0.3474**	**–1.3983**	*0.2749*
Condylon medial (L)	**–0.7729**	**–0.8551**	**0.5884**	**0.5884**	**–1.3955**	**–1.3200**	**0.2443**	**–1.4029**
Condylon lateral (L)	0.0588	0.0669	**0.4530**	**0.4530**	–0.0948	–0.0660	–0.1211	–0.1137
Mandibular foramen (L)	*–0.1578*	*–0.1501*	–0.0310	–0.0310	**–0.4135**	–0.1154	**–0.4518**	**–0.5055**
Mandibular foramen (R)	–0.0908	*–0.1584*	**–0.3432**	**–0.3432**	*–0.2536*	*–0.2413*	*–0.2675*	*–0.2661*
M3-lateral posterior (L)	–0.0631	–0.0789	**0.5405**	**0.5405**	*–0.2241*	*–0.2489*	*–0.2452*	*–0.2716*
M3-lateral posterior (R)	*0.2286*	*0.1974*	**1.0348**	**1.0348**	0.0213	0.0157	0.0038	–0.0056
M1M2 lateral (L)	*0.1781*	*0.1640*	**0.6065**	**0.6065**	–0.0065	–0.0270	–0.0217	–0.0462
M1M2 lateral (R)	–0.0860	–0.0628	**0.3406**	**0.3406**	**–0.4628**	**–0.3485**	**–0.3469**	**-0.3778**
CP3 lateral (R)	*–0.2290*	*–0.2020*	0.0696	0.0696	**–0.5577**	**–0.5415**	**–0.6697**	**–0.6833**
CP3 lateral (L)	0.0665	0.0914	**0.5026**	**0.5026**	–0.1306	–0.1262	*–0.1501*	–0.1468
Mental foramen (R)	**–0.4002**	*–0.1847*	**–0.9968**	**–0.9968**	**–0.6075**	**–0.7322**	**–0.6367**	**–0.7859**
Mental foramen (L)	**–0.4711**	**–0.4646**	**–0.9352**	**–0.9352**	NR	NR	NR	NR
Coronion (L)	*0.2252*	*0.2366*	**0.5418**	**0.5418**	0.1066	0.1085	0.0866	0.0928
Coronion (R)	0.0589	0.0480	**0.3684**	**0.3684**	–0.0420	–0.0662	–0.0697	–0.0803
Ramus-a (R)	0.1165	0.1147	*0.2853*	*0.2853*	0.0068	–0.0009	–0.0046	–0.0143
Ramus-a (L)	*0.2185*	*0.2170*	**0.3651**	**0.3651**	0.0906	0.0913	0.0817	0.0770
Ramus-p (R)	*0.2626*	*0.2531*	**0.5859**	**0.5859**	0.1163	0.0895	0.0940	0.0698
Ramus-p (L)	0.0661	0.0647	**0.3943**	**0.3943**	–0.0533	–0.0649	–0.0693	–0.0809
Sigmoid notch (R)	*0.2204*	*0.2262*	**0.8613**	**0.8613**	0.1201	0.0958	0.0963	0.0711
Sigmoid notch (L)	*0.2085*	*0.2244*	**0.6433**	**0.6433**	0.0578	0.0949	0.0358	0.0771
Linguale	*0.2191*	*0.2313*	**0.8063**	**0.8063**	0.0186	0.0282	0.0105	0.0027
Alveolus-p (L)	0.1127	0.1035	**0.4710**	**0.4710**	–0.0393	–0.0656	–0.0519	–0.0840
Alveolus-p (R)	0.1294	0.1415	**0.4371**	**0.4371**	–0.0196	0.0042	–0.0307	–0.0141
Gonion (R)	0.1350	0.1288	0.0266	0.0266	0.0317	0.0250	0.0077	0.0125
Gonion (L)	0.0549	0.0474	0.1231	0.1231	–0.0414	–0.0476	–0.0555	–0.0580

Notes: CMP1 = comparison point; M1 = HMH 0 smooth; M2 = HMH 0; M3 = HMH -500 smooth; M4 = HMH -500; M5 = HMH 562 smooth; M6 = HMH 562; M7 = HMH 634 smooth; M8 = HMH 634; NR = No Result. Gap distances for points above the 0.3 mm tolerance are indicated in italics, and those above the 0.15 median are indicated in bold. See also Supplemental Data.

of differential post-processing techniques may be warranted. When obtaining CT, laser, structured light, et cetera from websites and digital repositories, it is important that post-processing methods—or stages—be thoroughly identified, understood, and communicated and that these data be provided with each (see Boyer et al. [2017] for a recent review of MorphoSource; see Lebrun and Orliac [2017] for a recent review of MorphoMuseuM). In cases of 3D data, it is best to use the original files where possible (e.g., .tiff stacks, analyze files, DICOMs, etc.), as opposed to simply posting processed models/meshes. This would ensure that models and meshes can be rendered in a manner that yields consistent outputs for a specific project (Stock et al. 2020). For example, a project that is focused on dentition may use different thresholding techniques compared to that of a project focused on mandibular bone, femur, pelvis, et cetera.

2D Sectioning (2D Compare)

Although it is an important first step, the complex variability for two or more specimens identified through the first comparison (3D compare) requires two-dimensional sectioning, where gap distances can be further scrutinized, illustrated, and clarified. The contribution of the 2D compare results may be of particular importance prior to the application of semilandmarks (Bookstein 1991; Gunz et al. 2005) and sliding semilandmarks used to analyze the morphological variability among specific, well-defined curves (Bookstein 1997; Bookstein et al. 1999). The 2D compare sections illustrate specific areas of topology between the model and the mesh that are potentially problematic. For example, the 2D comparisons illustrate that areas of highly complex morphology may not be suitable locations for landmarks in a mixed-method

https://doi.org/10.1017/aap.2021.18 Published online by Cambridge University Press

dataset. Following identification of post-processing tools that result in the lowest gap distance between meshes and sections, landmark and semilandmark constellations can be refined.

Comparison Points

Identifying comparison points that should *not* be used as positions for landmarks or semilandmarks is as important as identifying those *to* use, given that the mesh topology in some regions will likely be better suited for a mixed-method approach than others. Those placed in areas of complex geometry—particularly areas with deeper structures associated with dentition, mental foramina, and fractures/breaks—deviate most (similar to results found in the 2D and 3D compare analyses). This could reflect the fact that surface scanning is limited to surface topography, whereas CT scans also capture elements of internal morphology. However, it is noteworthy that an analysis of a fully intact mandible may result in measures for comparison points on both condyles that are within tolerance, similar to those on the intact right condyle.

With this in mind, it is acknowledged that comparison points would not normally be placed on a broken specimen; instead, that area of the mesh would be virtually reconstructed (Benazzi et al. 2009; Godinho and O'Higgins 2017; Gunz et al. 2009; White 2015; Zollikofer and Ponce de Leon 2005), mirrored (Couette and White 2010), or otherwise treated as missing (Arbour et al. 2014; Couette and White 2010; Neubauer et al. 2012; Senck et al. 2013). However, placement of landmarks on the broken neck of the left condyle in this study provides interesting insights into potential problems associated with the application of comparison points—or landmarks—for mixed-method studies of complex geometric structures. Perhaps not surprisingly, these results suggest that CT scans may be better suited for analyses of deeper crevices (dentition), cranial sutures, foramina, fractures, and other biological structures at the point of transition from external to internal morphology. This finding is similar to that of Stock and colleagues (2020), who emphasized the importance of precise processing techniques when viewing complex anatomy, including the epiphyseal plates of subadult materials. The implications here are that the use of 3D scans or low thresholding that artificially "bloat" models may not pick up on the finer details, leading to erroneous biological interpretations. The current study did not specifically test how varying threshold levels or post-processing would affect results in an actual comparative study. Such analyses would be important avenues of future research. Additional avenues of research could involve investigating areas of "noise," including the use of varying post-processing techniques in combination with different scanners on a single item (e.g., utilizing two different CT scanners or two different 3D surface scanners).

These results represent one approach to identifying variation in mixed-methods datasets and demonstrate the need to compare data produced using different collection and post-processing methods prior to analysis. The comparative methodological approach can be tailored to aid in the gradual refinement of post-processing workflows when used for a single scanner coupled with omnifarious post-processing methods, algorithms, and settings used to collect, process, and model 3D scan data (see Selden 2017:22–23, Figure 2; Selden and Jones 2021; Selden, Means et al. 2018: Figure 4). To fully comprehend the complexities of the results, it is recommended that data be compared prior to formal analyses, allowing analysts to identify and further scrutinize specific areas of meshes that may prove problematic. Additional studies that compare modeling applications for skeletal objects (e.g., an entire cranium or post-cranial elements), cultural materials (e.g., ceramics, lithics; sensu Selden 2018a, 2018b, 2019, 2021; Selden, Dockall et al. 2018; Selden et al. 2020), and proposed curve and patch elements associated with the addition and incorporation of semilandmarks or sliding semilandmarks will add important insights to the gradual identification of those processing techniques most appropriate for a wider range of mixed-method studies.

CONCLUSION

Comparative studies of 3D data processed using different hardware and software are necessary to comprehend the ambiguity introduced through the use of different post-processing methods. This is of particular import when the models and/or meshes used were produced for another analysis, perhaps with very different goals and data-collection protocols. Scan data curated in digital archives or databases warrant additional scrutiny because contextual and scan-specific metadata are neither standardized nor required (see Davies et al. 2017; Niven and Richards 2017), and too often these details are not included in the description or summary. Although it may be tempting to quickly download and import 3D mesh data generated for another study, it is best to request the unprocessed data and spend the time necessary to identify the post-processing methods that are best suited to the research question. Note that the successful identification of a post-processing workflow that achieves the smallest gap distance/deviation in one study may not represent the correct—or most appropriate—choice for another study, given that variable research questions tend to focus on different elements of mesh topology.

For analyses that employ a mixed-method approach using 3D data from digital repositories, websites, or other investigators, the tests needed to identify specific post-processing protocols will depend on the research design and question. In most cases, it is best to begin by identifying post-processing protocols that result in the most consistent whole-object variability across the mesh sample using 3D comparisons that provide a general overview of areas that may not compare well across the sample, and therefore may need to be avoided in a landmark-based geometric morphometric study. The analysis of 2D sections could be used to investigate potential challenges associated with a specific curve (archaeology) or biological feature (anthropology) as a means of determining whether or not it is suitable for semilandmark placement. Finally, the use of comparison points provides a means of assessing variation at specific locations on the mesh in advance of formal analysis to determine whether or not those locations are suitable for landmarks or other point-based measurements.

Acknowledgments

We express our gratitude to the Department of Anthropology at the University of Colorado Boulder for the requisite permissions and access needed to generate the scans of the mandibles, and to Bernard K. Means and Bonny Ford for their useful comments on an earlier draft. Further thanks go to Ramesh Karki for assistance in CT scanning at the Anschutz Medical Campus and to Charles Musiba for facilitating various aspects of this research project. Additional thanks go to Paul Sandberg and Austin Lawrence, who helped to locate samples in the Wadi Halfa collection, as well as to Erik Ordaz, who helped with abstract translation.

https://doi.org/10.1017/aap.2021.18 Published online by Cambridge University Press

Data Availability Statement

All 3D data used in this analysis are digitally curated on Zenodo @ CERN (DOI:10.5281/zenodo.817449) and are embargoed for a period of five years from the most recent submission that employs them.

Supplemental Material

Supplemental material for this article is available on Zenodo, DOI: https://doi.org/10.5281/zenodo.817449.

Supplemental Data. Mesolithic mandible UCB-6B36-B11-2-15904-M from Sudan; curated in the collections at the University of Colorado at Boulder. Data were collected with a Creaform GoSCAN20. Additional data include CT scans produced using variable processing methods.

REFERENCES CITED

Adams, Dean C., F. James Rohlf, and Dennis E. Slice
2013 A Field Comes of Age: Geometric Morphometrics in the 21st Century. *Hystrix: The Italian Journal of Mammalogy* 24:7–14. DOI:10.4404/hystrix-24.1-6283.

Algee-Hewitt, Bridget F. B., and Amber D. Wheat
2016 The Reality of Virtual Anthropology: Comparing Digitizer and Laser Scan Data Collection Methods for the Quantitative Assessment of the Cranium. *American Journal of Physical Anthropology* 160:148–155. DOI:10.1002/ajpa.22932.

Allison, Penelope
2008 Dealing with Legacy Data - An Introduction. *Internet Archaeology* 24. DOI:10.11141/ia.24.8.

Arbour, Jessica H., Caleb M. Brown, and Shinichi Nakagawa
2014 Incomplete Specimens in Geometric Morphometric Analyses. *Methods in Ecology and Evolution* 5:16–26. DOI:10.1111/2041-210x.12128.

Balzeau, Antoine, Isabelle Crevecoeur, Hélène Rougier, Alain Froment, Emmanuel Gilissen, Dominique Grimaud-Hervé, Philippe Mennecier, and Patrick Semal
2010 Applications of Imaging Methodologies to Paleoanthropology: Beneficial Results Relating to the Preservation, Management and Development of Collections. *Comptes Rendus Palevol* 9:265–275. DOI:10.1016/j.crpv.2010.07.006.

Benazzi, Stefano, Ekarterina Stansfield, Ottmar Kullmer, Luca Fiorenza, and Giorgio Gruppioni
2009 Geometric Morphometric Methods for Bone Reconstruction: The Mandibular Condylar Process of Pico della Mirandola. *The Anatomical Record* (*Hoboken*) 292:1088–1097. DOI:10.1002/ar.20933.

Bookstein, Fred L.
1991 *Morphometric Tools for Landmark Data: Geometry and Biology*. Cambridge University Press, Cambridge.
1997 Landmark Methods for Forms without Landmarks: Localizing Group Differences in Outline Shape. *Medical Image Analysis* 1:225–243.

Bookstein, Fred, Katrin Schfer, Hermann Prossinger, Horst Seidler, Martin Fieder, Chris Stringer, Gerhard W. Weber, *et al.*
1999 Comparing Frontal Cranial Profiles in Archaic and Modern Homo by Morphometric Analysis. *The Anatomical Record* 257:217–224. DOI:10.1002/(sici)1097-0185(19991215)257:6<217::aid-ar7>3.0.co;2-w.

Bookstein, Fred L., Dennis E. Slice, Philipp Gunz, and Philipp Mitteroecker
2004 Anthropology Takes Control of Morphometrics. *Collegium Antropologicum* 28:121–132.

Boyer, Doug M., Gregg F. Gunnell, Seth Kaufman, and Timothy M. McGeary
2017 MorphoSource: Archiving and Sharing 3-D Digital Specimen Data. *Paleontological Society Papers* 22:157–181. DOI:10.1017/scs.2017.13.

Bruno, Fabio, Stefano Bruno, Giovanna De Sensi, Maria-Laura Luchi, Stefania Mancuso, and Maurizio Muzzupappa
2010 From 3D Reconstruction to Virtual Reality: A Complete Methodology for Digital Archaeological Exhibition. *Journal of Cultural Heritage* 11:42–49. DOI:10.1016/j.culher.2009.02.006.

Budzik, Grzegorz, Jan Burek, Anna Bazan, and Paweł Turek
2016 Analysis of the Accuracy of Reconstructed Two Teeth Models Manufactured Using the 3DP and FDM Technologies. *Strojniški vestnik - Journal of Mechanical Engineering* 62. DOI:10.5545/sv-jme.2015.2699.

Butaric, Lauren N.
2015 Differential Scaling Patterns in Maxillary Sinus Volume and Nasal Cavity Breadth among Modern Humans. *Anatomical Record* 298:1710–1721. DOI:10.1002/ar.23182.

Chirchir, Habiba, Christopher B. Ruff, Juho-Anti Junno, and Richard Potts
2017 Low Trabecular Bone Density in Recent Sedentary Modern Humans. *American Journal of Physical Anthropology* 162:550–560. DOI:10.1002/ajpa.23138.

Coleman, Mark N., and Matthew W. Colbert
2007 Technical Note: CT Thresholding Protocols for Taking Measurements on Three-Dimensional Models. *American Journal of Physical Anthropology* 133:723–725. DOI:10.1002/ ajpa.20583.

Copes, Lynn E., and William H. Kimbel
2016 Cranial Vault Thickness in Primates: Homo Erectus Does Not Have Uniquely Thick Vault Bones. *Journal of Human Evolution* 90:120–134. DOI:10.1016/j.jhevol.2015.08.008.

Couette, Sébastien, and Jess White
2010 3D Geometric Morphometrics and Missing-Data: Can Extant Taxa Give Clues for the Analysis of Fossil Primates? *Comptes Rendus Palevol* 9:423–433. DOI:10.1016/j.crpv.2010.07.002.

Davies, Thomas G., Imran A. Rahman, Stephan Lautenschlager, John A. Cunningham, Robert J. Asher, Paul M. Barrett, Karl T. Bates, et al.
2017 Open Data and Digital Morphology. *Proceedings of the Royal Society B: Biological Sciences* 284:20170194. DOI:10.1098/rspb.2017.0194.

Douglass, Mattjew, Dennis Kuhnel, Matthew Magnani, Luke Hittner, Michael Chodoronek, and Samantha Porter
2017 Community Outreach, Digital Heritage and Private Collections: A Case Study from the North American Great Plains. *World Archaeology* 49:1–16. DOI:10.1080/00438243.2017.1309299.

Evgenikou, V., and A. Georgopoulos
2015 Investigating 3D Reconstruction Methods for Small Artifacts. *International Archives of the Photogrammetry, Remote Sensing and Spatial Information Sciences* XL-5/W4:101–108. DOI:10.5194/isprsarchives-XL-5-W4-101-2015.

Fourie, Zacharias, Janalt Damstra, Peter O. Gerrits, and Yijin Ren
2011 Evaluation of Anthropometric Accuracy and Reliability Using Different Three-Dimensional Scanning Systems. *Forensic Science International* 207:127–134. DOI:10.1016/j.forsciint.2010.09.018.

Franklin, Daniel, Lauren Swift, and Ambika Flavel
2016 "Virtual Anthropology" and Radiographic Imaging in the Forensic Medical Sciences. *Egyptian Journal of Forensic Sciences* 6:31–43. DOI:10.1016/j.ejfs.2016.05.011.

Friess, Martin
2012 Scratching the Surface? The Use of Surface Scanning in Physical and Paleoanthropology. *Journal of Anthropological Sciences* 90:7–31. DOI:10.4436/jass.90004.

Galland, Manon, Denis P. Van Gerven, Noreen Von Cramon-Taubadel, and Ron Pinhasi
2016 11,000 Years of Craniofacial and Mandibular Variation in Lower Nubia. *Scientific Reports* 6:31040. DOI:10.1038/srep31040.

Georgopoulos, A., C. Ionnidis, and A. Valanis
2010 Assessing the Performance of a Structured Light Scanner. *International Archives of Photogrammetry, Remote Sensing and Spatial Information Sciences* 38:250–255.

Godinho, Ricardo M., and Paul O'Higgins
2017 Virtual Reconstruction of Cranial Remains: The H. Heidelbergensis, Kabwe 1 Fossil. In *Human Remains: Another Dimension: The Application of Imaging to the Study of Human Remains*, 1st ed., edited by David Errickson and Tim Thompson, pp. 135–147. Academic Press, London.

Greene, Ddavid Lee, and George Armelagos
1972 *The Wadi Halfa Mesolithic Population*. Research Report Number 11, Department of Anthropology, University of Massachusetts, Amherst.

https://doi.org/10.1017/aap.2021.18 Published online by Cambridge University Press

Gunz, Philipp, and Philipp Mitteroecker
2013 Semilandmarks: A Method for Quantifying Curves and Surfaces. *Hystrix: The Italian Journal of Mammalogy* 24:103–109. DOI:10.4404/hystrix-24.1-6292.
Gunz, Philipp, Philipp Mitteroecker, and Fred L. Bookstein
2005 Semilandmarks in Three Dimensions. In *Modern Morphometrics in Physical Anthropology*, edited by Dennis E. Slice, pp. 73–98. Plenum Publishers, New York.
Gunz, Philipp, Philipp Mitteroecker, Simon Neubauer, Gerhard W. Weber, and Fred L. Bookstein
2009 Principles for the Virtual Reconstruction of Hominin Crania. *Journal of Human Evolution* 57:48–62. DOI:10.1016/j.jhevol.2009.04.004.
Isler, Volkan, Bradford Wilson, and Ruzena Bajcsy
2006 Building a 3D Virtual Museum of Native American Baskets. *Third International Symposium on 3D Data Processing, Visualization, and Transmission*, pp. 954–961. DOI:10.1109/3dpvt.2006.38.
Katz, David, and Martin Friess
2014 Technical Note: 3D from Standard Digital Photography of Human Crania: A Preliminary Assessment. *American Journal of Physical Anthropology* 154:152–158. DOI:10.1002/ajpa.22468.
Koppe, Thomas, and Hiroshi Nagai
1995 On the Morphology of the Maxillary Sinus Floor in Old World Monkeys: A Study Based on Three-Dimensional Reconstructions of CT Scans. In *Proceedings of the 10th International Symposium on Dental Morphology*, edited by Ralf Johannes Radlanski and Herbert Renz, pp. 423–427. C. & M. Brünne, Berlin.
Koppe, Thomas, and K.-U. Schumacher
1992 Untersuchungen zum Pneumatisationsgrad des Viscerocranium beim Menschen und bei den Pongiden. *Acta anatomica Nipponica* 67:725–734.
Kuzminsky, Susan C., and Megan S. Gardiner
2012 Three-Dimensional Laser Scanning: Potential Uses for Museum Conservation and Scientific Research. *Journal of Archaeological Science* 39:2744–2751. DOI:10.1016/j.jas.2012.04.020.
Lebrun, Renaud, and Maëva J. Orliac
2017 MorphoMuseuM: An Online Platform for Publication and Storage of Virtual Specimens. *Paleontological Society Papers* 22:183–195. DOI:10.1017/scs.2017.14.
Li, Yadong, and Peihua Gu
2004 Free-Form Surface Inspection Techniques State of the Art Review. *Computer-Aided Design* 36:1395–1417. DOI:10.1016/j.cad.2004.02.009.
Mahmoud, Dalia, Abdallah Khali, and Mohammed Younes
2015 Optimization of the Longitudinal Resolution of a Structured Light Shape Reconstruction System, a DOE Approach. *International Journal of Precision Engineering and Manufacturing* 16:1935–1939. DOI:10.1007/s12541-015-0251-6.
Márquez, Samuel, and Jeffrey T. Laitman
2008 Climatic Effects on the Nasal Complex: A CT Imaging, Comparative Anatomical, and Morphometric Investigation of *Macaca mulatta* and *Macaca fascicularis*. *Anatomical Record* 291:1420–1445. DOI:10.1002/ar.20785.
Means, Bernard K.
2015 Promoting a More Interactive Public Archaeology: Archaeological Visualization and Reflexivity through Virtual Artifact Curation. *Advances in Archaeological Practice* 3:235–248. DOI:10.7183/2326-3768.3.3.235.
2017 A Digital Passport to the Past: The "Accidental" Public Archaeology of the Virtual Curation Laboratory. *Public Archaeology* 16:1–9. DOI:10.1080/14655187.2016.1258916.
Menéndez, Lumila Paula
2017 Comparing Methods to Assess Intraobserver Measurement Error of 3D Craniofacial Landmarks Using Geometric Morphometrics through a Digitizer Arm. *Journal of Forensic Sciences* 62:741–746. DOI:10.1111/1556-4029.13301.
Minetola, P., L. Iuliano, and F. Calignano
2015 A Customer Oriented Methodology for Reverse Engineering Software Selection in the Computer Aided Inspection Scenario. *Computers in Industry* 67:54–71. DOI:10.1016/j.compind.2014.11.002.
Montgomery, William M., Peter S. Vig, Eedward V. Staab, and Stephen R. Matteson
1979 Computed Tomography: A Three-Dimensional Study of the Nasal Airway. *American Journal of Orthodontics* 76:363–375. DOI:10.1016/0002-9416(79)90223-9.
Neubauer, Simon, Philipp Gunz, Gerhard W. Weber, and Jean-Jacques Hublin
2012 Endocranial Volume of *Australopithecus africanus*: New CT-Based Estimates and the Effects of Missing Data and Small Sample Size. *Journal of Human Evolution* 62:498–510. DOI:10.1016/j.jhevol.2012.01.005.
Niven, Kieron, and Julian D. Richards
2017 The Storage and Long-Term Preservation of 3D Data. In *Human Remains: Another Dimension: The Application of Imaging to the Study of Human Remains*, edited by David Errickson and Tim Thompson, pp. 175–184. Academic Press, San Diego.
Obeidat, Suleiman M., and Shivakumar Raman
2008 An Intelligent Sampling Method for Inspecting Free-Form Surfaces. *International Journal of Advanced Manufacturing Technology* 40:1125–1136. DOI:10.1007/s00170-008-1427-3.
Poniatowska, Malgorzata
2012 Deviation Model Based Method of Planning Accuracy Inspection of Free-Form Surfaces Using CMMs. *Measurement* 45:927–937. DOI:10.1016/j.measurement.2012.01.051.
Prossinger, Hermann, Horst Seidler, Lothar Wicke, Dave Weaver, Wolfgang Recheis, Chris Stringer, and Gerd B. Müller
2003 Electronic Removal of Encrustations inside the Steinheim Cranium Reveals Paranasal Sinus Features and Deformations, and Provides a Revised Endocranial Volume Estimate. *Anatomical Record. Part B, New Anatomist* 273:132–142. DOI:10.1002/ar.b.10022.
Rae, Todd C., and Thomas Koppe
2002 3D Imaging and Measurement in Studies of Cranial Pneumatization. In *Three-Dimensional Imaging in Paleoanthropology and Prehistoric Archaeology*, Actes du XIVème Congrès UISPP, edited by Bertrand Marfart and Hervé Delingette, pp. 11–16. BAR International Series 1049. British Archaeological Reports, Oxford.
Robinson, Christopher, and Claire E. Terhune
2017 Error in Geometric Morphometric Data Collection: Combining Data from Multiple Sources. *American Journal of Physical Anthropology* 164:62–75. DOI: https://doi.org/10.1002/ajpa.23257.
Schwartz, Gary T., J. Francis Thackeray, Cynthia Reid, and J. F. van Reenan
1998 Enamel Thickness and the Topography of the Enamel-Dentine Junction in South African Plio-Pleistocene Hominids with Special Reference to the Carabelli Trait. *Journal of Human Evolution* 35:523–542. DOI:10.1006/jhev.1998.0239.
Selden, Robert Z., Jr.
2017 Asymmetry of Caddo Ceramics from the Washington Square Mound Site: An Exploratory Analysis. *Digital Applications in Archaeology and Cultural Heritage* 5:21–28. DOI:10.1016/j.daach.2017.04.003.
2018a A Preliminary Study of Smithport Plain Bottle Morphology in the Southern Caddo Area. *Bulletin of the Texas Archeological Society* 89:63–89.
2018b Ceramic Morphological Organisation in the Southern Caddo Area: Quiddity of Shape for Hickory Engraved Bottles. *Journal of Archaeological Science: Reports* 21:884–896. DOI:10.1016/j. jasrep.2018.08.045.
2019 Ceramic Morphological Organisation in the Southern Caddo Area: The Clarence H. Webb Collections. *Journal of Cultural Heritage* 35:41–55. DOI:10.1016/j.culher.2018.07.002.
2021 Louisiana Limitrophe: An Iterative Morphological Exegesis of Caddo Bottle and Biface Production. In *Ancestral Caddo Ceramic Traditions*, edited by Duncan P. McKinnon, Jeffrey S. Girard, and Timothy K. Perttula, pp. 258–276. Louisiana State University Press, Baton Rouge.
Selden Robert Z., Jr., John E. Dockall, C. Britt Bousman, and Timothy K. Perttula
2021 Shape as a Function of Time + Raw Material + Burial Context? An Exploratory Analysis of Perdiz Arrow Points from the Ancestral Caddo Area of the American Southeast. *Journal of Archaeological Science: Reports* 37:102916. DOI:10.1016/j.jasrep.2021.102916.
Selden, Robert Z., Jr., John E. Dockall, and Morgane Dubied
2020 A Quantitative Assessment of Intraspecific Morphological Variation in Gahagan Bifaces from the Southern Caddo Area and Central Texas. *Southeastern Archaeology* 39:125–145. DOI:10.1080/0734578x.2020.1744416.
Selden, Robert Z., Jr., John E. Dockall, and Harry J. Shafer
2018 Lithic Morphological Organisation: Gahagan Bifaces from the Southern Caddo Area. *Digital Applications in Archaeology and Cultural Heritage* 10. DOI:10.1016/j.daach.2018.e00080.

https://doi.org/10.1017/aap.2021.18 Published online by Cambridge University Press

Selden, Robert Z., Jr., and Bradford M. Jones
2021 Reverse Engineering a Bronze Cannon from the *La Belle* Shipwreck. *Historical Archaeology* 55:290–299. DOI:10.1007/s41636-020-00280-2.
Selden, Robert Z., Jr., Bernard K. Means, Edward G. Iglesias, and Kreg Mosier
2018 Morphological Variation in Three-Dimensional Printed Replicas. *CRHR Research Reports* 4:Article 3. Electronic document, https://scholarworks.sfasu.edu/crhr_research_reports/vol4/iss1/3/, accessed August 17, 2021.
Selden, Robert Z., Jr., Bernard K. Means, Jon C. Lohse, Charles Koenig, and Stephen L. Black
2014 Beyond Documentation: 3D Data in Archaeology. *Texas Archeology* 58:20–24.
Selden, Robert Z., Jr., Timothy K. Perttula, and Michael J. O'Brien
2014 Advances in Documentation, Digital Curation, Virtual Exhibition, and a Test of 3D Geometric Morphometrics. *Advances in Archaeological Practice* 2:64–79. DOI:10.7183/2326-3768.2.2.64.
Senck, Sascha, Fred L. Bookstein, Stefano Benazzi, Johann Kastner, and Gerhard W. Weber
2015 Virtual Reconstruction of Modern and Fossil Hominoid Crania: Consequences of Reference Sample Choice. *Anatomical Record* 298:827–841. DOI:10.1002/ar.23104.
Senck, Sascha, Michael Coquerelle, Gerhard W. Weber, and Stefano Benazzi
2013 Virtual Reconstruction of Very Large Skull Defects Featuring Partly and Completely Missing Midsagittal Planes. *Anatomical Record* 296:745–758. DOI:10.1002/ar.22693.
Shearer, Brian M., Siobhán B. Cooke, Lauren B. Halenar, Samantha L. Reber, Jeannette E. Plummer, Eric Delson, and Melissa Tallman
2017 Evaluating Causes of Error in Landmark-Based Data Collection Using Scanners. *PLoS ONE* 12:e0187452. DOI:10.1371/journal.pone.0187452.
Sholts, S. B., L. Flores, P. L. Walker, and S. K. T. S. Wärmländer
2011 Comparison of Coordinate Measurement Precision of Different Landmark Types on Human Crania Using a 3D Laser Scanner and a 3D Digitiser: Implications for Applications of Digital Morphometrics. *International Journal of Osteoarchaeology* 21:535–543. DOI:10.1002/oa.1156.
Shott, Michael
2014 Digitizing Archaeology: A Subtle Revolution in Analysis. *World Archaeology* 46:1–9. DOI:10.1080/00438243.2013.879046.
Slice, Dennis E.
2007 Geometric Morphometrics. *Annual Review of Anthropology* 36:261–281. DOI:10.1146/annurev.anthro.34.081804.120613.
Spoor, Fred, Nathan Jeffery, and Frans Zonneveld
2000 Imaging Skeletal Growth and Evolution. In *Development, Growth and Evolution: Implications for the Study of the Hominid*, edited by Paul O'Higgins and Martin J. Cohn, pp. 123–161. Academic Press, London.
Spoor, C. Fred, Frans W. Zonneveld, and Gabriele A. Macho
1993 Linear Measurements of Cortical Bone and Dental Enamel by Computed Tomography: Applications and Problems. *American Journal of Physical Anthropology* 91:469–484. DOI:10.1002/ajpa.1330910405.
Stalling, Detlev, Malte Westerhoff, and Hans-Christian Hege
2005 Amira: A Highly Interactive System for Visual Data Analysis. In *The Visualization Handbook*, edited by Charles D. Hansen and Chris R. Johnson, pp. 749–767. Elsevier Butterworth–Heinemann, Burlington, Massachusetts. DOI:10.1016/b978-012387582-2/50040-x.
Stephen, Alexander J., Peter K. Wegscheider, Andrew J. Nelson, and James P. Dickey
2015 Quantifying the Precision and Accuracy of the MicroScribe G2X Three-Dimensional Digitizer. *Digital Applications in Archaeology and Cultural Heritage* 2:28–33. DOI:10.1016/j.daach.2015.03.002.
Stock, Michala K., Heather M. Garvin, Louise K. Corron, Cortney N. Hulse, Laura E. Cirillo, Alexandra R. Klales, Kerri L. Colman, and Kyra E. Stull
2020 The Importance of Processing Procedures and Threshold Values in CT Scan Segmentation of Skeletal Elements: An Example Using the Immature Os Coxa. *Forensic Science International* 309:110232. DOI:10.1016/j.forsciint.2020.110232.
Stull, Kyra E., Meredith L. Tise, Zabiullah Ali, and David R. Fowler
2014 Accuracy and Reliability of Measurements Obtained from Computed Tomography 3D Volume Rendered Images. *Forensic Science International* 238:133–140. DOI:10.1016/j.forsciint.2014.03.005.
Tocheri, Matthew W.
2009 Laser Scanning: 3D Analysis of Biological Surfaces. In *Advanced Imaging in Biology and Medicine*, edited by Christoph W. Sensen and Benedikt Hallgrímsson, pp. 85–101. Springer, Berlin. DOI:10.1007/978-3-540-68993-5_4.
Tzou, Chieh-Han, Nicole M. Artner, Igor Pona, Alina Hold, Eva Placheta, Walter G. Kropatsch, and Manfred Frey
2014 Comparison of Three-Dimensional Surface-Imaging Systems. *Journal of Plastic, Reconstructive and Aesthetic Surgery* 67:489–497. DOI:10.1016/j.bjps.2014.01.003.
Ullrich, C. G., E. F. Binet, M. G. Sanecki, and S. A. Kieffer
1980 Quantitative Assessment of the Lumbar Spinal Canal by Computed Tomography. *Radiology* 134:137–143. DOI:10.1148/radiology.134.1.7350593.
Wachowiak, Melvin J., and Basiliki Vicky Karas
2013 3D Scanning and Replication for Museum and Cultural Heritage Applications. *Journal of the American Institute for Conservation* 48:141–158. DOI:10.1179/019713609804516992.
Weber, Gerhard W.
2015 Virtual Anthropology. *American Journal of Physical Anthropology* 156:22–42. DOI:10.1002/ajpa.22658.
Weber, Gerhard W., and Fred L. Bookstein
2011 *Virtual Anthropology: A Guide to a New Interdisciplinary Field*. Springer-Verlag, Vienna.
Weyrich, T., M. Pauly, R., Keiser, S. Heinzle, S. Scandella, and M. Gross
2004 Post-Processing of Scanned 3D Surface Data. In *Eurographics Symposium on Point-Based Graphics*, edited by M. Alexa and S. Rusinkiewicz, pp. 85–94. Eurographics Association, Geneva, Switzerland.
White, Suzanna
2015 Virtual Archaeology: The NextEngine Desktop Laser Scanner. *Archaeology International* 18:41–44. DOI:10.5334/ai.1804.
Wong, F. S. Y., K. B. Chuah, and P. K. Venuvinod
2006 Automated Inspection Process Planning: Algorithmic Inspection Feature Recognition, and Inspection Case Representation for CBR. *Robotics and Computer-Integrated Manufacturing* 22:56–68. DOI:10.1016/j.rcim.2005.02.005.
Yogi, Muldani Hendrawan, Yuwana M. Yatna, and Sri Raharno
2014 Development of Computer Aided Inspection Planning (CAIP) Application in on Machine Measurement Operation (OMM) Operations for Box Primitive Features: Generating Inspection Codes. *Applied Mechanics and Materials* 660:889–893. DOI:10.4028/www.scientific.net/AMM.660.889.
Zelditch, Miriam Leah, Donald L. Swiderski, and H. David Sheets
2012 *Geometric Morphometrics for Biologists: A Primer*. 2nd ed. Academic Press, Waltham, Massachusetts.
Zollikofer, Christoph P., and Marcia Ponce de Leon
2005 *Virtual Reconstruction: A Primer in Computer-Assisted Paleontology and Biomedicine*. Wiley, New York.
Zonneveld, F., C. Spoor, and J. Wind
1989 The Use of the CT in the Study of the Internal Morphology of Hominid Fossils. *Medicamundi* 34:117–128.

AUTHOR INFORMATION

Robert Z. Selden Jr. ■ Heritage Research Center and Department of Biology, Stephen F. Austin State University, Nacogdoches, TX, USA; Cultural Heritage Department, Jean Monnet University, Saint-Étienne, France (zselden@sfasu.edu, corresponding author)

Lauren N. Butaric ■ Department of Anatomy, Des Moines University, Des Moines, IA, USA

Kersten Bergstrom ■ Department of Anthropology, Texas A&M University, College Station, TX, USA; School of Biological Sciences, Washington State University Tri-Cities, Richland, WA, USA

Dennis Van Gerven ■ Department of Anthropology, University of Colorado, Boulder, CO, USA

https://doi.org/10.1017/aap.2021.18 Published online by Cambridge University Press